HCN-HNC isomerization in oscillating fields

K.T. Mushir Ul Hasan

A dissertation submitted for the partial fulfillment of
BS-MS dual degree in Science

Indian Institute of Science Education and Research Mohali

April 2017

Certificate of Examination

This is to certify that the dissertation titled **HCN-HNC isomerization in oscillating fields** submitted by **Mr. K.T. Mushir Ul Hasan (Reg. No. MS12047)** for the partial fulfillment of BS-MS dual degree programme of the Institute, has been examined by the thesis committee duly appointed by the Institute. The committee finds the work done by the candidate satisfactory and recommends that the report be accepted.

Prof. K.S. Viswanathan Dr. K.R. Shamasundar Dr. P. Balanarayan (Supervisor)

Dated: April 21, 2017

Declaration

The work presented in this dissertation has been carried out by me with Dr. P. Balanarayan at the Indian Institute of Science Education and Research Mohali. This work has not been submitted in part or in full for a degree, a diploma, or a fellowship to any other university or institute. Whenever contributions of others are involved, every effort is made to indicate this clearly, with due acknowledgement of collaborative research and discussions. This thesis is a bonafide record of original work done by me and all sources listed within have been detailed in the bibliography.

K.T. Mushir Ul Hasan
(Candidate)

Dated: April 21, 2017

In my capacity as the supervisor of the candidate's project work, I certify that the above statements by the candidate are true to the best of my knowledge.

Dr. P. Balanarayan
(Supervisor)

Acknowledgements

First of all, I would like to express my sincere gratitude to Dr P. Balanarayan for providing me with an opportunity to work in the lab and for his constant support throughout the duration of the project. I would also like to thank my thesis committee members, Prof. K.S. Viswanathan and Dr K.R. Shamasundar for giving their valuable suggestions to work. I am grateful to my parents for their guidance, encouragement and support. I would also like to extend my gratitude to my friends for making these five years a merry ride. I am thankful to all my lab members, Naveen, Prashant, Abhijeet, Nitin, Prateek, Mishu and Deepraj for helpful discussions and making the time spent in the lab a pleasurable experience. Finally, I thank IISER Mohali for all the facilities and DST-INSPIRE for the financial support.

K.T. Mushir Ul Hasan

"All our knowledge begins with the senses, proceeds then to the understanding, and ends with reason. There is nothing higher than reason."

Immanuel Kant

Contents

List of Figures

List of Tables

Abbreviations

a.u.	**a**tomic **u**nits
KH	**K**ramers **H**enneberger
KHA	**K**ramers **H**enneberger **A**pproximation
IRC	**I**ntrinsic **R**eaction **C**oordinate
TDSE	**T**ime **D**ependent **S**chrödinger **E**quation
ITP	**I**maginary **T**ime **P**ropagation
DVR	**D**iscrete **V**ariable **R**epresentation

Physical Constants

Speed of Light	c	=	$2.997\ 924\ 58 \times 10^{8}\ ms^{-1}$
Reduced Planck's constant	$\hbar$	=	$1.054\ 571\ 80 \times 10^{-34}\ Js$
Charge of an electron	e	=	$1.602\ 176\ 62 \times 10^{-19}\ C$

Dedicated to my Parents and my Brother.

Abstract

The present work deals with the study of change in dynamics observed for a double well potential (HCN-HNC isomerization) in the Kramers-Henneberger frame under the influence of periodic driving. This change in dynamics gives us an insight into the chemistry of barriers in reaction pathways, namely the transition state. Along with the nuclear dynamics, preliminary investigations has also been performed on the electronic structure of HCN under the influence of oscillating fields.

Chapter 1

Introduction

Over the past few years, studies on chemistry in the presence of high-intensity high-frequency oscillating fields have gained momentum because of many interesting phenomena that occur under these conditions. Back when laser development was in its initial stages, people carried out plenty of theoretical studies on systems in the presence of oscillating fields. With the development of strong-field lasers, it has been possible for researchers to now investigate several effects exhibited by atoms and molecules in the presence of super-intense fields in the laboratory. The strength of such fields dealt with is usually of the order of 10^{12} W cm^{-2} or more. Exposing atomic or molecular systems to such high fields gives rise to much non-linear effects which can not be understood in the framework of perturbation theory. As a result, laser physics saw the development of various methods in order to accomodate the observations from numerical/experimental studies.

1.1 Historical background

One of the phenomena that have been investigated extensively over the past two or three decades is atomic stabilization,i.e., the atom tends to stabilize in high-intensity fields instead of getting ionized completely. Gersten and Mittleman[1] in 1976 proposed that beyond a critical value of laser intensity, the electron tends to stabilize

due to its quiver motion in the presence of high-intensity high-frequency oscillating fields. Stabilization could not be explained in the traditional perturbative framework because the strength of the external electric field is almost equal to that of the internal electric field of the atom/molecule[5]. The phenomena of atomic stabilization were studied extensively by Gavrila and co-workers with the Hydrogen atom as their system of interest[3].

1.2 Adiabatic stabilization

Stabilization has been known to be of mainly two types - Adiabatic Stabilization(or Kramers-Henneberger Stabilization) and dynamic stabilzation. According to this mechanism, in the high-intensity high-frequency regime, there is a significant reconstruction of the energy structure and the eigenstates. Kramers-Henneberger stabilization is primarily attributed to the formation of a 'dressed potential' at high laser strengths. To understand this stabilization mechanism, one has to delve into the KH framework which will be discussed in the upcoming section. The 'Adiabatic theorem'[6] in quantum mechanics states that "*For a slowly varying Hamiltonian, the instantaneous eigenstates of the Hamiltonian will continuously evolve into the corresponding eigenstates at a later time*". If the laser envelope is allowed to change adiabatically, the population in the initial bound state can be adiabatically transferred to the corresponding KH bound state. Stabilization achieved under these conditions is known as adiabatic stabilization.

1.3 Hamiltonian for a particle in an electromagnetic field

The Lagrangian for a particle in an electromagnetic field is given by the following equation (neglecting the magnetic field contributions)[7]:

$$L = \frac{p^2}{2m} + \frac{e}{c}(\dot{\vec{q}}.\vec{A}) - e\phi \tag{1.1}$$

where '$\vec{A}$' is the vector potential and 'ϕ' is the scalar potential.

From Lagrangian's equations of motion, the canonical momentum is defined as:

$$\frac{\partial L}{\partial \dot{q}} = m\vec{v} + \frac{e}{c}\vec{A} = \vec{p} \tag{1.2}$$

The classical Hamiltonian is given by

$$H = mv^2 - L \tag{1.3}$$

Substituting for the values of 'L' from equation (1.1) and 'v' from equation (1.2) results in the following expression for the classical Hamiltonian,

$$H = \frac{1}{2m}(\vec{p} - \frac{e}{c}\vec{A})^2 + e\phi \tag{1.4}$$

1.4 Kramers-Henneberger transformation

As mentioned earlier, to understand the dynamics of an atom in the super-intense laser field, one has to switch to KH frame. This transformation was first introduced by Henneberger[2] and its use was advanced by Gavrila and co-workers[3] to understand the dynamics of the Hydrogen atom in high-frequency fields. The transformation involves a change of frame of reference and introduces a time-dependent shift in the argument of the potential. The new potential thus formed has a characteristic double well shape which results in the dichotomous nature of the time-dependent wavefunction.

The Schrödinger equation for a Hydrogen atom, ignoring relativistic effects, in the presence of an electromagnetic field in the semi-classical dipole approximation is:

$$\frac{1}{2m}\left[\frac{\hbar}{i}\vec{\nabla} - \frac{e}{c}\vec{A}(t)\right]^2 \psi(\vec{r},t) + V(\vec{r})\psi(\vec{r},t) = i\hbar\frac{\partial}{\partial t}\psi(\vec{r},t) \tag{1.5}$$

Perturbative approaches have not been successful in elucidating the process underlying adiabatic stabilization. As a result, methods have had to resort to non-perturbative

treatments. The quiver motion exhibited by the electron in the presence of an electromagnetic field can be best represented in an accelerated frame of reference, popularly known as the Kramers-Henneberger(KH) frame. The change of frame of reference can be brought forth by performing a simple unitary transformation on the electronic wavefunction:

$$\Psi(\vec{r},t) = \hat{\Omega}\psi(\vec{r},t) \tag{1.6}$$

where '$\hat{\Omega}$' is defined as

$$\hat{\Omega} = exp\left[\frac{i}{\hbar}\int_{-\infty}^{t}\left\{\frac{i\hbar e}{mc}\vec{A}(t').\vec{\nabla} + \frac{e^2}{2mc^2}(\vec{A}(t'))^2\right\}dt'\right] = exp\left[\frac{i}{\hbar}\int_{-\infty}^{t}\hat{H}^t_{int}(t')dt'\right] \tag{1.7}$$

With the dipole approximation, '$\hat{\Omega}$' can be written as a product of two operators as shown below:

$$\hat{\Omega} = \hat{\Omega_1}\hat{\Omega_2} \tag{1.8}$$

where

$$\hat{\Omega_1} = exp\left[\frac{i}{\hbar}\int_{-\infty}^{t}\frac{i\hbar e}{mc}\vec{A}(t').\vec{\nabla}dt'\right]$$
$$\hat{\Omega_2} = exp\left[\frac{i}{\hbar}\int_{-\infty}^{t}\frac{e^2}{2mc^2}(\vec{A}(t'))^2dt'\right]$$

The new Schrödinger equation is given by

$$i\hbar\frac{\partial}{\partial t}|\Psi\rangle = \hat{H}|\Psi\rangle \tag{1.9}$$

Substituting for 'Ψ' and upon further simplification yields the following expression,

$$i\hbar\frac{\partial|\Psi\rangle}{\partial t} = \left[i\hbar\frac{\partial\Omega}{\partial t}\Omega^\dagger + \Omega\hat{H}\Omega^\dagger\right]|\Psi\rangle \tag{1.10}$$

Expanding the first term on the right hand side, we get

$$i\hbar\frac{\partial\Omega}{\partial t}\Omega^\dagger = i\hbar\left[\frac{\partial\Omega_1}{\partial t}\Omega_2\Omega_2^\dagger\Omega_1^\dagger + \Omega_1\frac{\partial\Omega_2}{\partial t}\Omega_2^\dagger\Omega_1^\dagger\right] \tag{1.11}$$

On applying Leibniz integral rule and the identity above to the first term of the right hand side in equation 1.11 results in the following reduced expression:

$$i\hbar\frac{\partial\Omega}{\partial t}\Omega^{\dagger} = -\frac{i\hbar e}{mc}\vec{A}(t).\vec{\nabla} - \frac{e^2}{mc^2}(\vec{A}(t)^2) + \Omega_1\Omega_2\hat{H}\Omega_2^{\dagger}\Omega_1^{\dagger} \tag{1.12}$$

Simplification of the above expression leads to the following,

$$i\hbar\frac{\partial\Omega}{\partial t} = \frac{-\hbar^2}{2m}\vec{\nabla}^2 + \Omega_1\hat{V}\Omega_1^{\dagger} \tag{1.13}$$

Since, Ω_1 has an exponential form, Baker-Haussdorf-Campbell[8] formula is applied on the second term in the above equation to finally yield the Schrödinger equation in the accelerated frame of reference,

$$i\hbar\frac{\partial\Psi}{\partial t} = -\frac{\hbar^2}{2m}\vec{\nabla}^2\Psi + \hat{V}(\vec{r}+\vec{\alpha})\Psi \tag{1.14}$$

1.5 Kramers-Henneberger Approximation and case of potentials under KHA

The potential part is space-translated by a factor of '$\alpha(\vec{t})$' after the Kramers-Henneberger transformation. This potential can now be expanded by a Fourier series which can be interpreted as a combination of time-independent and time dependent terms.

$$V(\vec{r}+\alpha(\vec{t})) = V_0 + \sum_{n=0}^{n=\infty} V_n\cos(n\tau) \tag{1.15}$$

where 'V_0^{KH}'(n=0,1,2,. . .) is given by

$$V_n^{KH} = \frac{1}{2\pi}\int_0^{2\pi} V(\vec{r}+\alpha(\vec{t}))\cos(n\tau)d\tau \tag{1.16}$$

At very high frequencies, under the Kramers-Henneberger Approximation(KHA), the sum of non-zero harmonics from the Fourier series expansion can be considered as a small perturbation. Therefore, the significant contribution comes from the zero-order harmonic part which is time independent and is responsible for the formation of stable

states at high frequencies. So, the Schrödinger equation under the KHA is given by:

$$-\frac{1}{2}\vec{\nabla}^2\Psi + V_0^{KH}\Psi = E^{KH}\Psi \tag{1.17}$$

1.5.1 Coulomb potential

The 1-D coulombic potential is given by the following expression and is shown by the red curve in Figure 1.1.

$$V(x) = -\frac{1}{|x|} \tag{1.18}$$

The zeroeth order KH transformed potential (blue curve in Figure 1.1) is therefore given by:

$$V_0^{KH} = -\frac{1}{2\pi}\int_0^{2\pi} \frac{d\phi}{|x + \vec{\alpha_o}\cos\phi|} \tag{1.19}$$

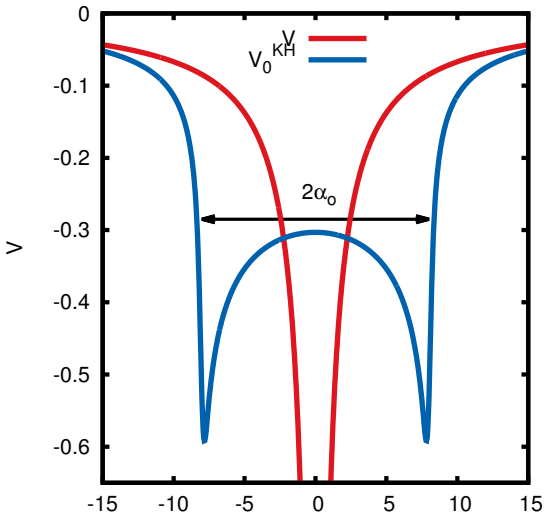

FIGURE 1.1: Coulomb potential and KH transformed potential

The splitting shown in Figure 1.1 is proportional to the value of α_o with the distance between two minimas being $2\alpha_o$.

1.5.2 Polynomial potentials - Symmetric double well

For a polynomial potential of the form:

$$V(x) = ax^4 - bx^2 \tag{1.20}$$

which is characterized by the presence of two minima at '$\pm\sqrt{\frac{b}{2a}}$', there is a significant difference in the dynamics in the presence of an oscillating field.

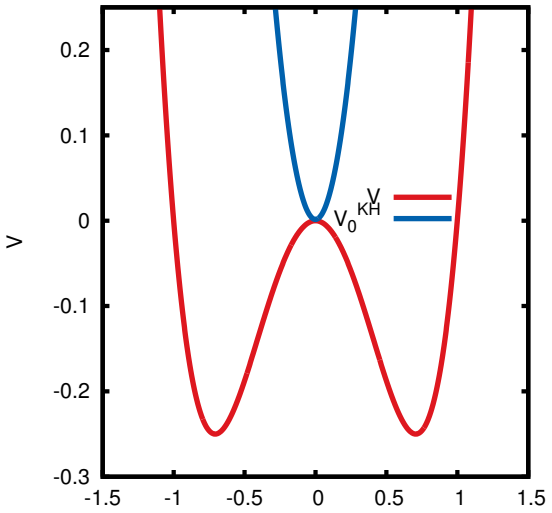

FIGURE 1.2: S-double well potential and KH transformed potential

As shown in Figure 1.2, there is an apparent change in dynamics from tunneling to that of a coherent one for which the wavefunction is centered on the origin [5].

1.6 Plan of thesis

Mostly, all the studies till now have only looked at atoms and the behaviour of electronic potentials in the presence of oscillating fields. The change in dynamics for a vibrational potential (discussed in the last section) can have new implications in the study of barriers in chemical reactions. As given in the previous section, the KH transformed potential has its minimum on top of the barrier indicating barrier stabilization. The goal of this work is to look at this interesting phenomenon and provide

a proper numerical framework for localizing molecular wavefunctions on top of the barrier. The plan of the work is therefore given as follows:

- Obtain parameters for a vibrational potential (in this case an asymmetric double well).
- Periodic driving of the asymmetric double well in the KH framework.
- Localizing the molecular wave packet on top of the barrier.
- Analysis of the system (like calculating ionization rates) in the presence of oscillating field.

References

[1] J.I. Gersten and M.H. Mittleman, *J. Phys. B* **9**, 2561 (1976).

[2] W.C. Henneberger, *Phys. Rev. Lett.* **21**, 838 (1968).
H.A. Kramers, *Collected scientific papers* (North-Holland, Amsterdam, 1956).

[3] M. Gavrila and J. Kaminski, *Phys. Rev. Lett.* **52**, 613 (1984).
M. Pont, N.R. Walet, M. Gavrila and C.W. McCurdy, *Phys. Rev. Lett.* **61**, 939 (1988).
M. Pont, N.R. Walet and M. Gavrila, *Phys. Rev. A* **41**, 477 (1990).

[4] Q. Su, A. Sanpera, and L. Roso-Franco, *Int. J. Mod. Phys. B* **8**, 1655 (1994).

[5] P.P. Corso and E. Persico, *J. Mod. Opt.* **42**, 2425 (1995).

[6] P. D. Robinson, Hypervirial theorems and perturbation theory in quantum mechanics, *Proc. R. Soc. London* **283**, 229237 (1965).

[7] John David Jackson, *Classical Electrodynamics* (Wiley, India, 2013).

[8] $e^{\hat{A}}\hat{B}e^{-\hat{A}} = \hat{B} + \left[\hat{A}, \hat{B}\right] + \frac{1}{2!}\left[\hat{A}, \left[\hat{A}, \hat{B}\right]\right] + \ldots$.

Chapter 2

Model one-dimensional potential for HCN-HNC isomerization

This isomerization reaction has been the subject of numerous theoretical as well as experimental studies. The reaction entails a linear more stable HCN isomerizing to a less stable linear HNC. The reaction proceeds through a triangular transition state structure. The asymmetric double well is formed as a result of migration of the Hydrogen atom from Carbon to Nitrogen which follows a semi-circular pathway with the Hydrogen tethered to the center-of-mass of CN moiety. Recently, several theoretical studies have been reported on the isomerization reaction in the presence of the laser. Sun et.al. have reported the laser-driven isomerization of HCN-HNC in the presence of an intense picosecond infrared laser with a particular emphasis on the importance of rotational excitation[1]. Dion et. al. numerically studied the isomerization reaction using two perpendicular IR pulses to show that it mainly proceeds through the bending mode of the molecule[2]. Recently, Mellau et. al. discussed localization of molecular wavefunctions on the saddle point of the HCN-HNC minimum energy path[11]. In the next chapter, analysis has been done to arrive at a similar result by localizing the wavepacket on top of the barrier in the presence of oscillating fields.

2.1 Asymmetric double well potential

In order to create the asymmetric double well, *ab initio* calculations were done to generate points along the intrinsic reaction coordinate at Hartree-Fock and correlated level of theories with different basis sets using standard electronic structure packages[3]. The step size used in the IRC calculation was 0.05 bohr a.m.u$^{1/2}$. The energies of critical geometries at different basis sets has been tabulated in Table 2.1.

TABLE 2.1: HF Energy of HCN, HNC and the TS at various basis sets

Basis set	HCN	HNC	TS
6-31G*	-92.87519	-92.85532	-92.79195
aug-cc-pvdz	-92.88843	-92.87196	-92.81264
aug-cc-pvtz	-92.91131	-92.89488	-92.83348
aug-cc-pvqz	-92.91691	-92.90063	-92.83908
aug-cc-pv5z	-92.91808	-92.90179	-92.84023
aug-cc-pv6z	-92.91823	-92.90019	-92.84038
coemd-3	-92.90739	-92.89259	-92.82869
coemd-ref	-92.91761	-92.90138	-92.83963
ano-rcc	-92.91838	-92.89753	-92.83593

Figure 2.1 depicts the IRC pathway at different basis sets. Going down the list of basis sets used, there is an increase in the number of basis functions used per atom. Despite, having lesser number of basis fucntions per atom with respect to augmented

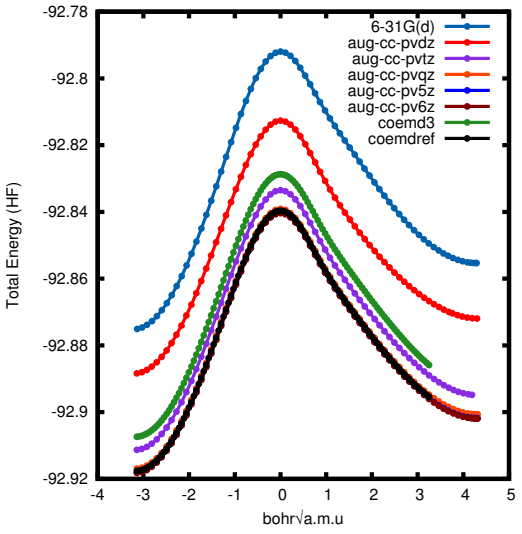

FIGURE 2.1: IRC plot at different basis sets

V5Z/V6Z[12], coemd-ref[13] proves to be an acceptable basis set.

A correlated single point calculation was later performed at CCSD(T) level of theory with coemd-ref as the basis set and the values of isomerization energy has been tabulated below in comparison to other works.

TABLE 2.2: Selected theoretical and experimental values for HCN-HNC isomerization energy

$\Delta E_o(cm^{-1})$	Method	ref
5100 ± 700	Ion-cyclotron resonance	Pau and Hehre[4] (1982)
5200 ± 300	Ion-molecule reaction	Hansel et al.[5] (1998)
5040 ± 350	CCSD(T)/ANO	Lee and Rendell[6] (1991)
5050	PES based on CCSD(T)/ANO	Bentley et al.[7] (1992)
5186 ± 50	CCSD(T) based PES	van Mourik et al.[8] (2001)
5140	CCSD(T)/cc-pVTZ	DePrince[9] and Mazziotti (2008)
5240	CCSDT(Q)/CBS with INT-MP2-F12	Vogiatzis et al.[10] (2014)
5081	CCSD(T)/coemd-ref	present work

A similar calculation was later done at a correlated level of theory(MP2) with coemd-ref as the basis set. The step size used was 0.05 bohr a.m.u$^{1/2}$. The points thus obtained were fitted using a curve fitting tool in MATLAB[14]. The fitting was a Gaussian type fit which was a combination of 8 terms.

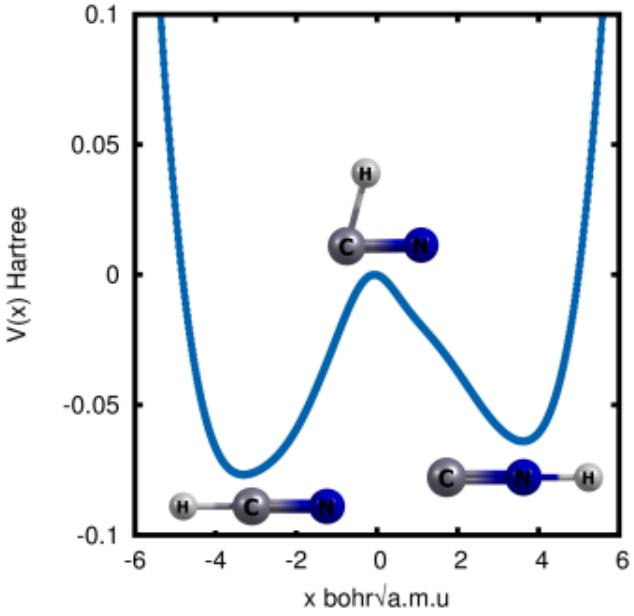

FIGURE 2.2: Fitted HCN-HNC asymmetric double well

The functional form of the potential is as follows:

$$V(x) = \sum_{n=1}^{n=8} a_i \exp\left[\left(\frac{x - b_i}{c_i}\right)^2\right] \tag{2.1}$$

The constants in the above expression has been tabulated below:

TABLE 2.3: Values of constants from the fit

a_1	-0.1147	b_1	-1.623	c_1	1.855
a_2	-0.01209	b_2	-1.359	c_2	0.7359
a_3	-85.74	b_3	8.892	c_3	16.2
a_4	-0.04037	b_4	0.6291	c_4	0.9549
a_5	-0.04029	b_5	-0.4389	c_5	0.8727
a_6	-66.93	b_6	-11.24	c_6	12.46
a_7	0.0005792	b_7	1.371	c_7	0.4781
a_8	-0.07134	b_8	1.532	c_8	1.429

Details of the fit are given below:

TABLE 2.4: Goodness of fit

SSE(Summed square of Residuals)	2.076e-06
R-square	1
Adjusted R-square	1
RMSE(Root Mean Square Error)	0.0001478

In the next chapter, the numerical results from the periodic driving of the asymmetric double well are presented.

References

[1] Z. Sun and Y. Zheng, *J. Phys. Chem. A* **119**, 2982 (2015).

[2] C. M. Dion, S. Chelkowski, A. D. Bandrauk, H. Umeda, and Y. Fujimura, *J. Chem. Phys.* **105**, 1083 (1996).

[3] M. J. Frisch, G. W. Trucks, H. B. Schlegel, G. E. Scuseria, M. A. Robb, J. R. Cheeseman, G. Scalmani, V. Barone, B. Mennucci, G. A. Petersson, H. Nakatsuji, M. Caricato, X. Li, H. P. Hratchian, A. F. Izmaylov, J. Bloino, G. Zheng, J. L. Sonnenberg, M. Hada, M. Ehara, K. Toyota, R. Fukuda, J. Hasegawa, M. Ishida, T. Nakajima, Y. Honda, O. Kitao, H. Nakai, T. Vreven, J. A. Montgomery, Jr., J. E. Peralta, F. Ogliaro, M. Bearpark, J. J. Heyd, E. Brothers, K. N. Kudin, V. N. Staroverov, T. Keith, R. Kobayashi, J. Normand, K. Raghavachari, A. Rendell, J. C. Burant, S. S. Iyengar, J. Tomasi, M. Cossi, N. Rega, J. M. Millam, M. Klene, J. E. Knox, J. B. Cross, V. Bakken, C. Adamo, J. Jaramillo, R. Gomperts, R. E. Stratmann, O. Yazyev, A. J. Austin, R. Cammi, C. Pomelli, J. W. Ochterski, R. L. Martin, K. Morokuma, V. G. Zakrzewski, G. A. Voth, P. Salvador, J. J. Dannenberg, S. Dapprich, A. D. Daniels, O. Farkas, J. B. Foresman, J. V. Ortiz, J. Cioslowski, and D. J. Fox *Gaussian 09, Revision C.01*, Gaussian, Inc., Wallingford CT, 2010.

M.W. Schmidt, K.K. Baldridge, J.A. Boatz, S.T. Elbert, M.S. Gordon, J.H. Jensen, S. Koseki, N. Matsunaga, K.A. Nguyen, S.J. Su, T.L. Windus, M. Dupuis and J.A. Montgomery, *J. Comput. Chem.* **14**, 1347 (1993).

[4] C.F. Pau and W.J. Hehre, *J. Phys. Chem.* **86**, 321 (1982).

[5] A. Hansel, Ch. Scheiring, M. Glantschnig, W. Lindinger and E.E. Ferguson, *J. Chem. Phys.* **109**, 1748 (1998).

[6] T.J. Lee and A.P. Rendell, *Chem. Phys. Lett.* **177**, 491 (1991).

[7] J.A. Bentley, J.M. Bowman, B. Gazdy, T.J. Lee and C.E. Dateo, *Chem. Phys. Lett.* **198**, 563 (1992).

[8] T. van Mourik, G.J. Harris, O.L. Polyansky, J. Tennyson, A.G. Cśaszár and P.J. Knowles, *J. Chem. Phys.* **115**, 3706 (2001).

[9] A.E. DePrince III and D.A. Mazziotti, *J. Phys. Chem. B* **112**, 16158 (2008).

[10] K.D. Vogiatzis, R. Haunschild and W. Klopper, *Theor. Chem. Acc.* **133**, 1446 (2014).

[11] G.C. Mellau, A.A. Kyuberis, O.L. Polyansky, N. Zobov and R.W. Field, *Sci. Rep.* **6**, 33068 (2016).

[12] T.H. Dunning, Jr. *J. Chem. Phys.* **90**, 1007 (1989).
R.A. Kendall, T.H. Dunning, Jr. and R.J. Harrison, *J. Chem. Phys.* **96**, 6796 (1992).
A.K. Wilson, T.v. Mourik and T.H. Dunning, Jr., *J. Mol. Struct.(THEOCHEM)* **388**, 339 (1997).

[13] J. Lehtola, P. Manninen, M. Hakala and K. Hmlinen, *J. Chem. Phys.* **137**, 104105 (2012).

[14] MATLAB and Statistics Toolbox Release R2013a, The MathWorks, Inc., Natick, Massachusetts, United States.

Chapter 3

Numerical results

The final one-dimensional asymmetric double well potential obtained from the last section is subjected to KH transformation for a characteristic value of laser intensity and frequency. Further analysis on the dynamics of stability in the presence of oscillating fields is presented.

3.1 Time averaged zeroeth-order KH potential

In the space-translated frame, the term describing the oscillating field is incorporated into the potential which can be written as $V(\vec{r}+\alpha(\vec{t}))$ where the quiver motion '$\alpha(\vec{t})$' can be represented by

$$\alpha(\vec{t}) = \frac{1}{c}\int_0^t A(\vec{t'})dt' \tag{3.1}$$

The KH potential, as explained earlier, can be expanded in a Fourier basis to give a sum of time-independent and time-dependent terms. Within the framework of KH approximation, the contribution of zeroeth-order harmonic is considered. Given below is a simple result obtained by integrating the space translated potential over a full cycle for various values of the quiver distance.

As shown in the Figure 3.1, for increasing value of the quiver distance, the dynamics goes from less tunneling type to a more tunneling one and finally to an stabilizing

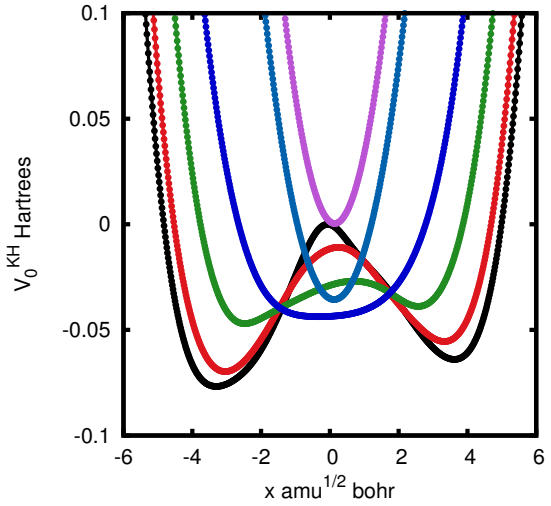

FIGURE 3.1: Variation of V_0^{KH} with increasing α_o.

type similar to that of a harmonic oscillator.

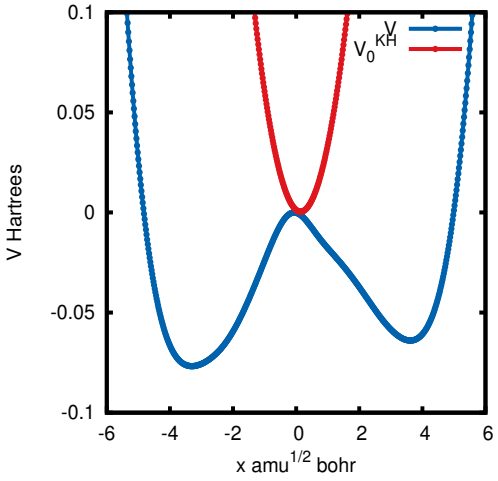

FIGURE 3.2: Zero-order harmonic at $\alpha_o = 5.635$ in a.u.

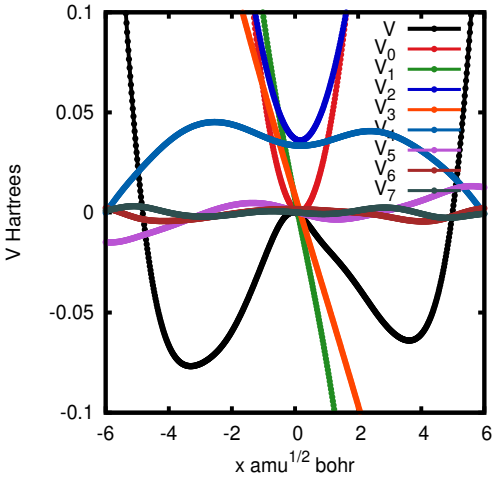

FIGURE 3.3: Non-zero harmonics at $\alpha_o = 5.635$ in a.u.

Figure 3.2 represents barrier stabilization which is clearly illustrated by the position of the minimum of the KH transformed potential right on top of the barrier of the asymmetric double well. The value of 'α_o' at which the minimum sits on top of the barrier is 5.635 a.u.. Figure 3.3 on the right side represents the non-zero harmonics in the Fourier series expansion upto seven terms for the same value of 'α_o'.

3.2 Higher-order corrections

The potential in the KH frame of reference for continuous wave laser field can be written as:

$$V^{KH}(x,t) = V(x - \alpha_o \cos \omega t) \tag{3.2}$$

In the limit of KH approximation, the transformed Hamiltonian depends only on '$\vec{\alpha_o}$'. To get a frequency dependence on field parameters, Ido gilary et. al.[1] came up with an alternate representation of the time-dependent Hamiltonian for strong-field driven systems using perturbation theory. In their work, the sum of non-zero harmonics is treated as a perturbation and the KH transformed Hamiltonian is subjected to another transformation.

$$V_{pert} = V^{KH}(x,t) - V_0^{KH} = \sum_{n\neq 0} V_n \exp(in\omega t) \tag{3.3}$$

The Hamiltonian in the accelerated frame of reference is given by:

$$H^{KH} = -i\hbar\frac{\partial}{\partial t} + \frac{\vec{p}^2}{2\mu} + V(x - \alpha_o \cos \omega t) \tag{3.4}$$

The transformation is done by introducing an alternate representaion of the wave-function which has the form:

$$\psi_i^{new} = \exp\left[\frac{i}{\hbar}\int^t \left[V^{KH}(x,t') - V_0^{KH}\right] dt'\right] \psi_i^{KH}(x,t) \tag{3.5}$$

The new Hamiltonian obtained after the above transformation thus is given by:

$$\hat{H}^{new}(x,t) = \hat{H}_0^{KH} - i\hbar\frac{\partial}{\partial t} + V^{new}(x,t) \tag{3.6}$$

where the new potential is

$$\begin{aligned} V^{new}(x,t) = &-\frac{1}{2\mu\omega^2}\left(\sum_{n\neq 0}\frac{f_n}{n}\exp(in\omega t)\right)^2 - \frac{\hbar}{2\mu\omega}\sum_{n\neq 0}\frac{1}{n}\frac{\partial f_n}{x}\exp(in\omega t) \\ &- \frac{\hbar}{\mu\omega}\sum_{n\neq 0}\frac{f_n}{n}\exp(in\omega t)\frac{\partial}{\partial x} \end{aligned} \tag{3.7}$$

In the above equation, the nth Fourier component of the force is defined by '$f_n(x) = -\frac{\partial V_n(x)}{\partial x}$,.

Application of perturbation theory to the newly transformed Hamiltonian provides a zero-order potential with direct dependence on field parameters:

$$V_0^{new}(x) = V_0^{KH} + \frac{1}{2\mu\omega^2}\sum_{n\neq 0}\frac{f_n(x)f_{-n}(x)}{n^2}. \tag{3.8}$$

The higher-order corrections to the zero-order KH energies has been obtained in the case of asymmetric double well and is depicted by the Figure 3.4 given below: This

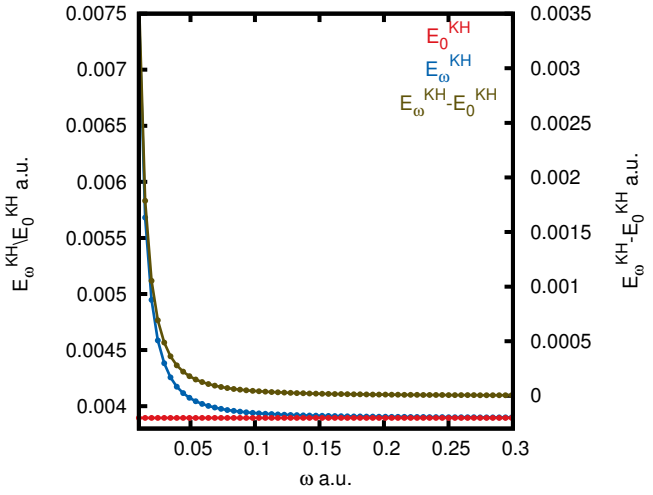

FIGURE 3.4: Zero-order and higher-order quasienergies obtained in the KH representation at maximum field amplitude of $\alpha_o = 5.635 a.u.$

result gives a frequency estimate of $\omega = 0.1$ $a.u.$ at which barrier stabilization can be realized. For further investigations, frequency $\omega = 0.05$ $a.u.$ has been selected which is proven to be a decent estimate with convergence of the order of 10^{-5} $a.u.$.

3.3 Time propagation - Nuclear dynamics

Describing the nuclear dynamics of the system in th oscillating frame involves solving the following Time-dependent Schrödinger equation (TDSE):

$$-i\frac{\partial}{\partial t}\psi(x,t) = \left[-\frac{1}{2}\frac{\partial^2}{\partial x^2} + V\left(x - \alpha_o\cos\omega t\right)\right]\psi(x,t) \tag{3.9}$$

where

$$\alpha_o = \frac{\epsilon}{\mu\omega^2}. \tag{3.10}$$

There is a considerable amount of mathematical complexity involved when it comes to obtaining exact analytical solutions of the TDSE. Since it's hard to integrate and find the solutions to the above equation directly, certain approximations have to be made which paves the way for numerical solution of the TDSE. One such method is to look at the evolution of the wavefunction using a time propagator. The propagator which has to satisfy certain properties is defined as:

$$U(t,0) = \exp\left[-\frac{i\hat{H}t}{\hbar}\right]. \tag{3.11}$$

3.3.1 Split-operator method

The goal is to evaluate the action of this unitary operator on the wavefunction at a given time. There are plenty of methods available for the evaluation of the above unitary time propagator. One such method which has been employed in the current work is called the 'Split-operator' method given by Feit et. al.[2] (1982) where the operator is approximated as a product of kinetic and potential energy terms:

$$\exp\left[-\frac{i\hat{H}\delta t}{\hbar}\right] \approx \exp\left[-\frac{i(\hat{T}+\hat{V})\delta t}{\hbar}\right] \approx \exp\left[-\frac{i\hat{T}\delta t}{\hbar}\right]\exp\left[-\frac{i\hat{V}\delta t}{\hbar}\right] \tag{3.12}$$

The above relation, as shown above, is highly approximate as both the kinetic energy and the potential energy operators do not commute with each other and therefore cannot be written as a product of their respective exponential terms. This approximate is accompanied by an error of order 'δt^2'. A symmetrized product as defined below can reduce the order of error to 'δt^3'and therefore is a much better approximation to the earlier result.

$$\exp\left[-\frac{i\hat{H}\delta t}{\hbar}\right] = \exp\left[-\frac{i\hat{V}\delta t}{2\hbar}\right]\exp\left[-\frac{i\hat{T}\delta t}{\hbar}\right]\exp\left[-\frac{i\hat{V}\delta t}{2\hbar}\right] + O(\delta t^3) \tag{3.13}$$

The numerical implementation of this technique involves representing the approximated unitary operator over a time interval $[0, t]$ and evaluating the action of the propagator in short discrete time intervals. Assessing the effect of the last term in the approximation is pretty straightforward as it just only involves multiplication of the potential operator on the wavefunction. After that, the resultant product is subject to a Fourier transform from coordinate representation to the momentum representation which in turn can be directly multiplied by the kinetic energy term. Later, an inverse Fourier transform is performed on this new product to be again multiplied by the potential operator. A schematic of the numerical implementation is given below:

$$\psi(x, t+\delta t) = \exp\left[-\frac{i\hat{V}\delta t}{2\hbar}\right] \xleftarrow{I.F.T} \exp\left[-\frac{i\hat{T}\delta t}{\hbar}\right] \xleftarrow{F.T} \exp\left[-\frac{i\hat{V}\delta t}{2\hbar}\right] \psi(x,t) \tag{3.14}$$

3.3.2 Imaginary Time Propagation(ITP)

To find the bound state in the presence of an oscillating field, ITP was implemented in the split-operator mechanism. ITP is a standard technique employed in determining bound states for any arbitrary given scalar potentials. The main crux is to replace the real time 't' by an imaginary time '$t = -i\tau$'. This transformation results in following form of the TDSE:[3]

$$\frac{\partial}{\partial\tau}\psi(x,\tau) = \hat{H}\psi(x,\tau) \tag{3.15}$$

The wavefunction at any imaginary time 'τ' can be defined as:

$$\psi(x,\tau) = \exp\left[-\tau\hat{H}\right]\psi(x,0) = \sum_n \exp\left[-\tau E_n\right] c_n\phi_n(x) \tag{3.16}$$

During the propagation, with increasing time, states with higher energies will die out and states with '$E_n < 0$' will tend to diverge. Re-normalization is carried out at every time step and subsequent iterations converge to give the ground state. For the propagation, following pulse sequence with an adiabtic smooth rise[4] was used:

$$\vec{\alpha(t)} = \begin{cases} \alpha_o \sin^2\left[\frac{\pi}{2}\frac{t}{t_{on}}\right]\sin\omega t, & 0 \le t \le t_{on} \\ \alpha_o \sin\omega t, & t \ge t_{on} \end{cases}$$

The parameters given in Table 3.1 were implemented in the pulse profile as described earlier for the propagation. The result of the ITP has been given in Figure 3.5. The

TABLE 3.1: Parameters for the pulse profile

Parameter	Values (in a.u.)
α_o	5.635
t_{on}	8000
ϵ_o	0.0140875
ω	0.05
n	1000000
t_{max}	10000

wavelength of the field used in this study comes out to be 911.6 nm which falls in the near-infrared (NIR) region. The initial wavepacket for this type of propagation can be

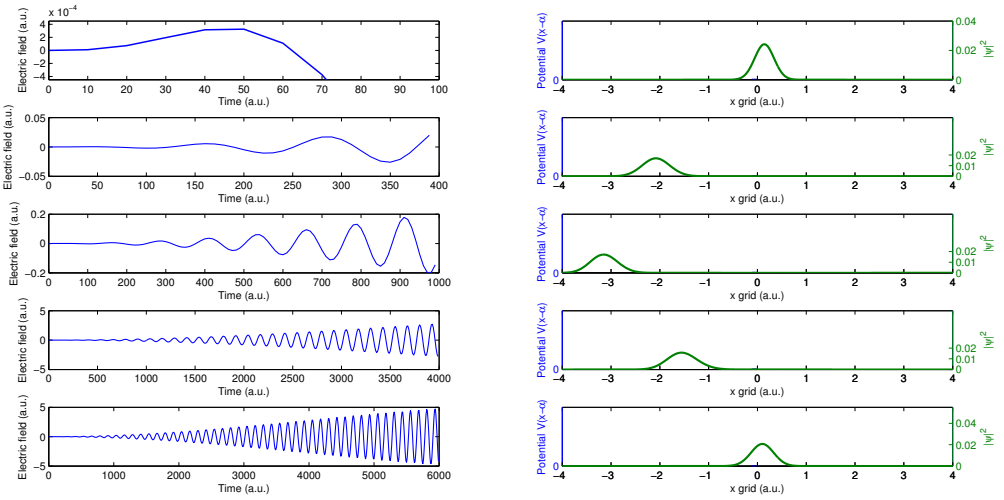

FIGURE 3.5: Evolution of the initial state with pulse progression at $I = 6.95 \times 10^{12} W cm^{-2}$ and $\omega = 1.36eV(911.6\ nm)$.

selected arbitrarily. Here, the wavepacket chosen was localized on the barrier. In the beginning, as the pulse is rising gradually, the wavepacket splits into two peaks which is tantamount to both wells of the asymmetric double well getting populated. In time, a stable wavepacket is localized in the HCN well. When the laser attains a continuous wave form, the wavepacket slowly starts shifting to the right with the result being it getting localized on the barrier which is characteristic of the KH transformed potential obtained for the HCN-HNC potential.

3.4 Ionization yield

The ionization of the system in the presence of oscillating fields was looked at the intensity and frequency for which stabilization has been described in the last section. Two methods in particulcar were employed in finding the yield which will be described in the follwing sections.

3.4.1 Frequency Corrected - Ammosov-Delone-Krainov model

This model of calculating tunneling rates was given as an improvement over the standard Ammosov-Delone-Krainov (ADK)[5]. The tunneling rate calculcated from FC-ADK[6] model is integrated over the whole pulse duration to obtain the ionization yield along the intrinsic reaction coordinate. The tunneling rate according to FC-ADK is given by:

$$\Gamma_{FC-ADK} = N_e \sqrt{\frac{3F_e}{\pi\kappa^3}\left(\frac{2}{\kappa}-1\right)}\frac{F_e}{8\pi}\left(\frac{4e\kappa^3}{\left(\frac{2}{\kappa}-1\right)F_e}\right)^{\frac{2}{\kappa}}\exp\left(-\frac{2\kappa^3}{3F_e}g(\gamma)\right) \tag{3.17}$$

where 'F_e' is the envelope fucntion of the electric field, '$\kappa = \sqrt{2I_p(x)}$'($I_p(x)$ is the ionization potential), '$\gamma = \frac{\kappa\omega}{F_e}$' and '$N_e$' is the number of active electrons.The function '$g(\gamma)$' given in the above equation has the following form:

$$g(\gamma) = \frac{3}{2\gamma}\left[\left(1+\frac{1}{2\gamma^2}\right)\operatorname{arcsin} h\gamma - \frac{\sqrt{1+\gamma^2}}{2\gamma}\right] \tag{3.18}$$

As the function '$g(\gamma) \approx 1$' in the limit '$\gamma << 1$', FC-ADK gets reduced to the standard ADK model. The ionization rate is calculated as:

$$Y(x) = 1 - \exp\left[-\int \Gamma\left[F_e(t), I_p(x)\right] dt\right]. \tag{3.19}$$

In case of the HCN-HNC asymmetric double well system, the envelope function used was the one defined in the last section and 'N_e' is taken to be two (as there are 2 electrons in the HOMO orbital for HCN). Koopmans' ionization potential was used as

'$Ip(x)$' in the above calculation. The following result was obtained for the ionization yield for different frequencies: From Figure 3.6, it is clear that no ionization is observed

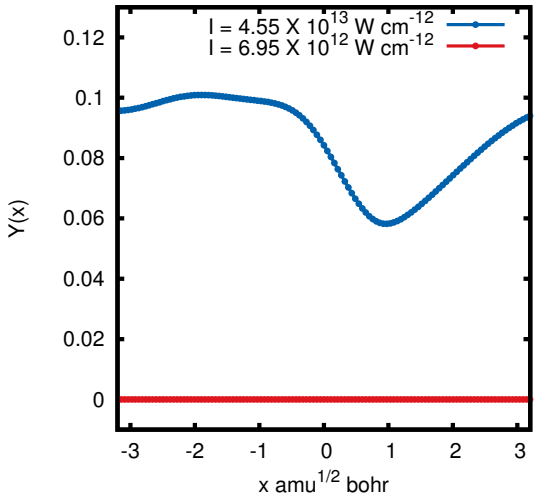

FIGURE 3.6: Ionization yield along the minimum energy path as calculated from FC-ADK model.

at $I = 6.95 \times 10^{12}\ Wcm^{-2}$ at which the barrier stabilization has been decribed for the asymmetric double well. As the intensity is slightly increased to $I = 4.55 \times 10^{13}\ Wcm^{-2}$, around 10% ionization is observed for HCN.

3.4.2 Ionization rates in strong field using Time-dependent Configuration Interaction and Complex Absorbing Potential

The second approach to calculating ionization rates is done using TDCIS-CAP[7] where the loss of electron density has been simulated using a Complex Absorbing Potenial(CAP). The form of the CAP used has been discussed by Santra et. al.[8]. The dynamics in the presence of electric field has been described by the following TDSE:

$$i\frac{\partial}{\partial t}\psi_{el}(t) = \hat{H}(t)\psi_{el}(t) \tag{3.20}$$

where '$\hat{H}(t)$', assuming the interaction between light and the system to be within the semi-classical dipole approximation and with CAP is:

$$\hat{H}(t) = \hat{H}_{el} - \vec{\mu}\vec{E(t)} - i\hat{V}^{absorb} \tag{3.21}$$

where 'μ' is the dipole operator, '$E(t)$' is the electric field term and '$\hat{V}^{absorb}$' is the complex absorbing potential. The time dependent wavefunction given in the TDSE above can be written as a linear combination of ground and excited field-free states with time dependent coefficients.

$$\psi(t) = \sum_i C_i(t)|\psi(t)\rangle \tag{3.22}$$

The TDSE can be re-written as:

$$i\frac{\partial}{\partial t}C_i(t) = \sum_j H_{ij}C_j(t) \tag{3.23}$$

where '$H_{ij} = \langle\psi_i|\hat{H}(t)|\psi_j\rangle$'. The time evolution of the coefficients of expansion is implemented numerically in the follwowing manner:

$$C(t+\delta t) = \exp\left[-iH\left(t+\frac{\delta t}{2}\right)\delta t\right]C(t). \tag{3.24}$$

The field-free wavefunctions for the HCN, HNC and the transition state was obtained using a time-dependent Configuration Interaction Singles calculation using the GAMESS[9] package. The pulse parameters given in the last section has been used in this study. The normalization of the wavefunction was plotted against the pulse duration. From Figure 3.7, it is depicted clearly that at the end of the pulse, of the TS survives and of HCN and HNC survives the duration of the pulse. There is a significant amount of population which survives the better part of the pulse for stabilization to occur.

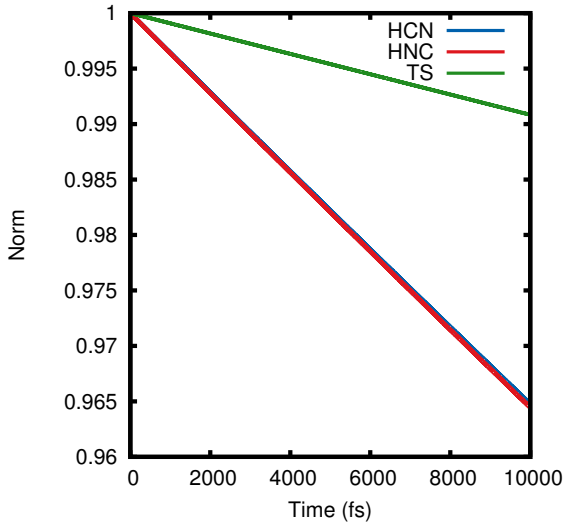

FIGURE 3.7: Strong field ionization rates for HCN, HNC and the TS for 'ϵ_o = 0.0140875 *a.u.*' and '$\omega = 0.05$ *a.u.*'

3.5 Electronic potential

A sample calculation for predicting the electronic structure of HCN in the presence of oscillating fields under the KHA. The black curve in Figure 3.8 shows the Coulomb

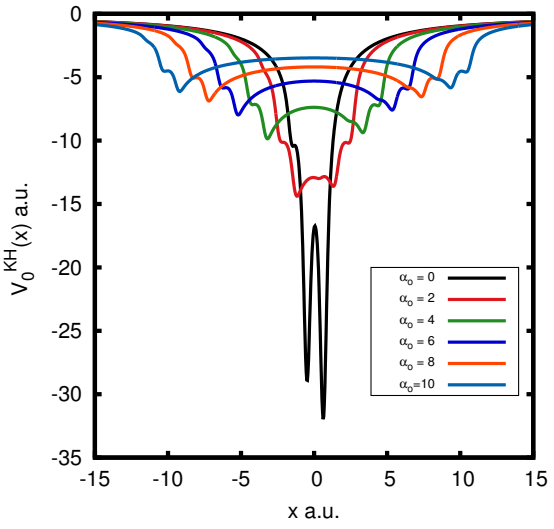

FIGURE 3.8: Electronic potential for increasing values of α_o.

plot of HCN with each peak representing the position of the respective atoms. The charge density is expressed with the depth of each of these peaks. With the application of KHA, each peak splits into two as shown earlier in the case of Coulomb potential and the individual contributions will add up to give a final potential as demonstrated

by the red curve at a particular value of α_o. The magnitude of splitting increases as the value of α_o is increased, and this is faithfully represented in Figure 3.8. In the case of the KH transformed potential, Carbon atom becomes more negative owing to the splitting of peaks. This effect results in a change of hybridization of the central atom from 'sp^3' to 'sp^2'. Using valence bond theory, since the central atom is 'sp^2' hybridised, the stable structure it can have will be bent which is essentially the transition state in the HCN-HNC isomerization pathway.

References

[1] Ido Gilary and Nimrod Moiseyev, *Phys. Rev. A* **66**, 063415 (2002).

[2] M.D. Feit, J.A. Fleck Jr., and A. Steiger, *J. Comp. Phys.* **47**, 412 (1982).

[3] Philipp Bader, Sergio Blanes and Fernando Casas, *J. Chem. Phys.* **139**, 124117 (2013).

[4] R. Dum, A. Sanpera, K. Suominen, M. Brewczyk, M. Kuś, K. Rzążewski and M. Lewenstein, *Phys. Rev. Lett.* **80**, 3899 (1998).

[5] M.V. Ammosov, N.B. Delone and V.P. Krainov, Sov. Phys. JETP **64**, 1191 (1986).

[6] J. Förster, Y.V. Vanne and A. Saenz, *Phys. Rev. A* **90**, 053424 (2014).

[7] P. Krause, J.A. Sonk and H.B. Schlegel, *J. Chem. Phys.* **140**, 174113 (2014).

[8] R. Santra and L.S. Cederbaum, *J. Chem. Phys.* **115**, 6853 (2001).

[9] M.W. Schmidt, K.K. Baldridge, J.A. Boatz, S.T. Elbert, M.S. Gordon, J.H. Jensen, S. Koseki, N. Matsunaga, K.A. Nguyen, S.J. Su, T.L. Windus, M. Dupuis and J.A. Montgomery, *J. Comput. Chem.* **14**, 1347 (1993).

Appendix A

Discrete Variable Representation

DVR is a powerful method mostly employed in solving the time-independent Schrödinger equation for a given potential. It is one of the grid-based methods used for obtaining eigenvalues and eigenvectors for a Hamiltonian. In this representation, the associated basis functions are localized about the discrete values of the variables and also the coordinate operators are assumed to be diagonal. DVR has become a versatile tool owing to its simplicity in evaluating kinetic energy matrix elements and the potential operator which requires no integral evaluations and its applications in molecular ro-vibrational spectroscopy and quantum dynamics. Following form of a simple one-dimensional DVR was given by Colbert and Miller[1].

The Kinetic energy operator in one-dimension is given by:

$$\hat{T} = -\frac{\hbar^2}{2m}\frac{d}{dx^2} \tag{A.1}$$

The coordinate 'x' is restricted on the interval (a, b) and the wavefunctions should vanish at the endpoints of the given interval. The grid points $\{x_i\}$ is calculated as:

$$x_i = a + i\frac{(b-a)}{N} \qquad i = 0, 1, 2...., N-1 \tag{A.2}$$

where 'N' is the number of grid points.

The functions associated with a uniform grid as given above are particle-in-a-box

[1]D.T. Colbert and W.H. Miller, *J. Chem. Phys.* **96**, 1982 (1991).

eigenfunctions:

$$\phi_n(x) = \sqrt{\frac{2}{b-a}} \sin\left[\frac{n\pi(x-a)}{b-a}\right] \tag{A.3}$$

where $n = 1, 2, ..., N-1$. There are only $N-1$ points in the interval and $N-1$ functions as it goes to '0' at the endpoints.

The kinetic energy thus can be represented in its DVR form as given below:

$$T_{ij} = \frac{\hbar^2}{2m}\delta x \sum_{n=1}^{N-1} \phi_n(x_i)\phi_n''(x_j) \tag{A.4}$$

$$= \frac{\hbar^2}{2m}\left(\frac{\pi}{b-a}\right)^2 \frac{2}{N} \sum_{n=1}^{N-1} n^2 \sin\left(\frac{n\pi i}{N}\right) \sin\left(\frac{n\pi j}{N}\right) \tag{A.5}$$

By summing over all the terms, the reduced form of the kinetic energy term can be written as:

$$T_{ij} = \frac{\hbar^2}{2m}\frac{(-1)^{i-j}}{(b-a)^2}\frac{\pi^2}{2}\left\{\frac{1}{\sin^2\left[\pi(i-j)/2N\right]} - \frac{1}{\sin^2\left[\pi(i+j)/2N\right]}\right\}, \quad i \neq j \tag{A.6}$$

$$T_{ij} = \frac{\hbar^2}{2m}\frac{1}{(b-a)^2}\frac{\pi^2}{2}\left\{\frac{(2N^2+1)}{3} - \frac{1}{\sin^2\left(\pi i/N\right)}\right\}, \quad i = j \tag{A.7}$$

In the interval $(-\infty, \infty)$, the grid spacing 'δx' requires that $N \longrightarrow \infty$. The final matrix representation in this interval is:

$$T_{ij} = \frac{\hbar^2}{2m\delta x^2}(-1)^{i-j} \begin{cases} \pi^2/3\ , & i = j \\ 2/(i-j)^2, & i \neq j \end{cases}$$

where $i = 0, \pm1, \pm2, \pm3, \ldots$.

A sample calculation was done on a model potential of the form:

$$V(x) = e^{-0.1x^2}\left(\frac{x^2}{2} - 0.8\right) \tag{A.8}$$

This potential holds only one bound state with $E = -0.2979596$ *Hartrees*. Given in Figure A.1 is a plot of the potential with the bound state.

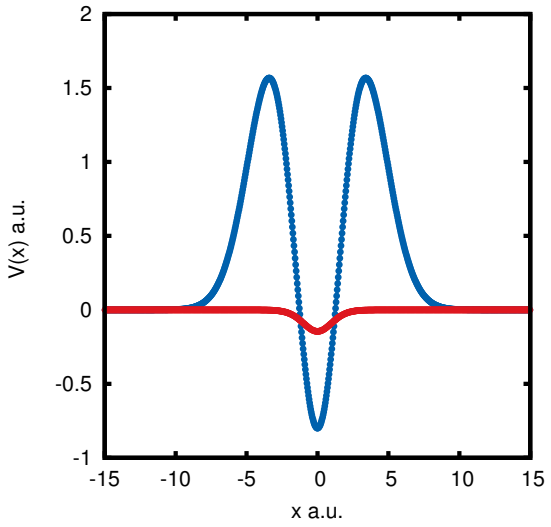

FIGURE A.1: Model Potential [Blue] and the bound state [Red]